



Optimization of the preparation conditions for cocoa shell-based activated carbon and its evaluation as salts adsorbent material

A. Y. León^{1,2} · J. R. Rincón¹ · N. Rodríguez³ · D. R. Molina⁴

Received: 4 April 2021 / Revised: 18 July 2021 / Accepted: 20 September 2021 / Published online: 7 October 2021
© Islamic Azad University (IAU) 2021

Abstract

Activated carbons from cocoa shell-based were obtained to evaluate their capacity as a salt adsorbent material (methylene blue and ferric chloride) an aqueous solution. The dry shell (cocoa shell precursor) was ground and classified into three particle sizes, 8–20, 40–60, and 80–120 + mesh, and with them activated carbons were obtained by a controlled thermochemical process using a 2³ factorial experiment design, with the surface area as the response variable, and the temperature (420–480 °C), impregnation ratio IR (1–1.5), and reaction time (30–120 min) as independent variables. The best preparation conditions were 480 °C, 1.5 (IR), and a reaction time of 30 min. From these conditions, three activated carbons with surface areas of 990, 1217, and 969 m²/g were prepared, and designated A, B, and C, respectively. Additionally, activated carbons presented characteristics of mesoporous structures. The adsorption analyses performed by UV–VIS showed that the adsorption efficiency of methylene blue (50 to 100 mg/L) and ferric chloride (100 to 250 mg/L) was B > C > A, and the removals of methylene blue and ferric chloride were from 97.1 to 89.8% and from 94.4 to 82.3%. FTIR spectroscopy analysis shows that the activated carbons contain abundant functional groups related to carboxylic acids and phenols. The experimental data were fitted to the Freundlich, Langmuir, and Temkin adsorption models. The Freundlich adsorption model obtained the lowest error values, followed by the Langmuir and Temkin adsorption models. The adsorption isotherms by adjusting the coefficient of determination (R²) and the sum of squared errors were classified.

Keywords Vegetable biomass · Thermogravimetry · Adsorption isotherms · UV–VIS spectroscopy

Introduction

In different industrial sectors such as textiles, mining, metallurgy, and oil, among others, large amounts of wastewater are generated, whose composition is highly varied and rich in toxic wastes and chemical substances (Jan et al. 2010; Rasalingam et al. 2014; Charles et al. 2016; Alkathiri et al. 2020). With increase in industrialization, the production of harmful organic and inorganic substances and heavy metals such as arsenic, cadmium, chromium, cobalt, copper, iron, lead, manganese, mercury, nickel, tin, and zinc has also increased (Pangeni et al. 2014; Chen et al. 2017a, b; Ma et al. 2017; Wołowiec et al. 2019; Deng et al. 2020; Egirani et al. 2020). Most of these substances are not biodegradable and act as species resistant to the environment, which causes ecological damage and unfavorable effects on the development of ecosystems and living beings.

Following environmental approaches, industries have been showing interest in developing new studies and methods for the treatment of their waters (Bhatti et al. 2011;

Editorial responsibility: Samareh Mirkia.

✉ A. Y. León
adanleon@uis.edu.co

- ¹ Grupo de Investigaciones en Corrosión GIC, Facultad de Ingenierías Físico Químicas, Universidad Industrial de Santander- UIS, A.A 678 Bucaramanga, Colombia
- ² Grupo de Recobro Mejorado, GRM, Facultad de Ingenierías Físico Químicas, Universidad Industrial de Santander- UIS, A.A 678 Bucaramanga, Colombia
- ³ Centro de Biotecnología & Agroindustria-ABC, Facultad de Ciencias, Universidad Industrial de Santander- UIS, A.A 678 Bucaramanga, Colombia
- ⁴ Laboratorio de Resonancia Magnética Nuclear, Facultad de Ciencias, Universidad Industrial de Santander- UIS, A.A 678 Bucaramanga, Colombia



Wang et al. 2015; Harsha et al. 2017). In general, water treatment involves physical methods followed by physicochemical methods. But, at this stage, it is not possible to remove all pollutants, especially dissolved organic compounds, heavy metals, and chemicals. Although there are technologies for treating produced water, these can involve high costs, long reaction times, and low efficiency for water with high concentrations of contaminants (Fakhru'l-Razi et al. 2009; Igunnu et al. 2014; Yousef et al. 2020). Conventional physical, chemical, and biological processes for wastewater decontamination are usually applied. Chemical treatment is applied to increase effluent quality by using coagulating and flocculating agents; however, it is less effective for substances with a high degree of solubility (Heiderscheidt et al. 2015; Pathania et al. 2017; Liu et al. 2019). Biological treatment depends on the chemical composition of the pollutants, nature, and microorganisms, and their growth affects the ability to degrade the species in the water. The selectivity of microorganisms is associated with the characteristics of the effluent and the process conditions, but the process is not very efficient to eliminate substances in effluents continuous, and short periods (Robinson et al. 2001; Panahi et al. 2018). Regarding the physical process, in the first separation stage and/or after chemical or biological treatments, the removal of solids, particles, and soluble substances can be conducted by precipitation, ion exchange, membrane filtration, electrochemical destruction, and ozonation, among others (Hameed et al. 2008; Shou et al. 2016; Agrawal et al. 2017).

Several studies have focused on adsorption methods using activated carbon of different materials such as wood, organic material, residual biomass, and polymers. Activated carbons have cavities or pores in their structure, and their content contributes to the quality of textural properties. These properties define the specific surface area of the material and confer adsorbent properties to remove toxic substances. In general, activated carbons from organic material with high carbon content are synthesized (Odubiyi et al. 2012; Fares et al. 2018; Meng et al. 2019; Yang et al. 2020; Valério et al. 2020). Lignocellulosic biomass is a sustainable feedstock, and its use which reduces the accumulation of residual biomass in the form of fruit peel, wood, and leaves is projected. Currently, one of the agroindustries that generate a large amount of lignocellulosic biomass in the department of Santander (Colombia) is the cocoa sector, since it is the largest cocoa producer with 42.1% equivalent. Colombia is the fifth largest cocoa producer worldwide and the third largest in Latin America, for which it projects production of 246,000 tons by 2021 (Ortiz et al. 2014; Sánchez et al. 2021). The cocoa industry economically exploits the seed (cocoa beans), which represents 10% of the weight of the fresh fruit, and in the manufacture of chocolate, its derivatives are used.

However, other by-products such as cocoa mucilage and shell are produced and represent about 75.7 and 85.9% of the total fruit on a wet basis (Afoakwa et al. 2013; Campos et al. 2018). The valorization of residual biomass such as cocoa shell plays an important role within the economic and environmental scheme. In addition, the high content of lignocellulosic biomass makes it an ideal precursor for the preparation of biomaterials.

The pretreatment of residual biomass represents one of the main technological challenges for the utilization and subsequent conversion into bioproducts with high added value such as activated carbons. Meanwhile, the characteristics of the valorization processes depend on the activation, pyrolysis conditions, and nature of the fluids of interest. Unlike many works reported in the bibliography, the present research work, as an innovative aspect, seeks to contribute to the sustainable socioeconomic development of the country by carrying out future projects on a pilot scale. In this way, an appropriate methodology for pretreatment and synthesis of activated carbons, it is possible to develop and commercialize adsorbent materials, based on the efficient management of biomass and the sustainable use of biodiversity and its ecosystemic services. The most important properties of adsorbents are the retention capacity and selectivity of the substances. Nonetheless, the concentration of the soluble pollutant (adsorbate), the pH of the solution, and the pollutant-adsorbent ratio are also important (Faria et al. 2008; Sotelo 2013). There is a wide variety of adsorbent materials of a carbonaceous nature, which greatly influences their porosity and surface area, and the multi-component separation properties. Activated carbons are materials with high adsorption capabilities, of which a large part is produced from organic waste, mainly of the lignocellulosic type. Furthermore, it has been established, through thermogravimetry and heat treatment tests, that a high percentage of the lignocellulosic material is transformed into activated carbon, while organic compounds such as cellulose and hemicellulose are converted into liquid products and gases. Thermogravimetric analysis to determine the kinetics of the pyrolysis process of materials is applied. Previously, kinetic models from various heating rates with values around 5, 10, 15, 20, and 40 °C/min are determined. However, the heating rates depend on the type of biomass. From the curve with a specific heating rate, it is essential to identify the degradation stages of the substances studied. In this way, it is possible to determine the abrupt changes and the temperature range of mass loss. Moreover, a low heating rate around 10 to 15 °C/min is recommended, because there is a significant exothermic difference between pyrolysis and in situ heterogeneous oxidation of biomass (Melgar et al.



2008; Manals et al. 2011; Saldarriaga et al. 2015; Han et al. 2016; Jo et al. 2017). The application and selectivity of activated carbons largely depends on the preparation conditions, and their chemical and textural properties (Wang et al. 2011; Díaz et al. 2013; Rivera et al. 2016; Oliveira et al. 2017; Aliakbari et al. 2018; Vuppaladadiyam et al. 2019). The use of biomass to prepare activated carbons has a positive impact on reducing organic waste. In numerous researches works, the use of activated carbons from vegetable biomass has been contemplated, due to their high efficiency in the removal of organic and inorganic compounds such as metals (White et al. 2011; Oyedun et al. 2014; Contescu et al. 2018; Cai et al. 2018; Priya et al. 2020). However, this efficiency depends on the nature of the vegetal material, reaction time, and chemical activation (Tejeda et al. 2014; Deliyanni et al. 2015; Yakout et al. 2016; Pak et al. 2016; Wahid et al. 2017).

To comply with the above, in this work, the cocoa shell precursor was used as raw material to produce activated carbon and evaluate its adsorption capacity with methylene blue and ferric chloride. Methylene blue is a cationic dye and is classified as organic salt. This dye is adapted in research due to its great potential to evaluate the quality of adsorbent materials (Ndolomingo et al. 2015). To obtain the best pyrolysis conditions, a 2³ factorial design was carried out using temperature, impregnation ratio, and reaction time as process variables. The quality of the carbons and the analysis of the adsorption isotherms were conducted by ATR-FTIR and UV-VIS spectroscopy. Finally, the results obtained in the experimental tests were fitted to the models of the adsorption isotherms from Freundlich, Langmuir, and Temkin.

Materials and methods

Materials

In this work, the shell from the cocoa fruit with a humidity of 83.43% by weight was selected. The biomass on a dry basis was selected due to its content of cellulose (30.84% by weight), hemicellulose (23.85% by weight), and lignin (28.35% by weight). The biomass activation was conducted with phosphoric acid (99.5%, Sigma-Aldrich) with impregnation ratio of 1 and 1.5 with respect to the cocoa shell. The pyrolysis tests were carried out in a horizontal Carbolite UN 110 reactor in an inert chamber with nitrogen grade 5. For the adsorption tests, the salts of methylene blue (99%, Sigma-Aldrich) and ferric chloride (99%, Sigma-Aldrich) were used.

Activated carbon preparation

Chemical composition of cocoa shell

Moisture content was determined by adding 1 g of initial biomass in a previously weighed capsule. Then, the capsule with the sample was placed in an oven with controlled temperature at 105 °C, for a period of 120 min. By weight difference, the biomass wet weight is reported until a constant weight is obtained. To determine the holocellulose content, about 2 g of dry biomass with known humidity and sieved in the 60–80 mesh range was weighed. The sample was treated by adding 150 ml of 1.5% sodium chlorite and 10 drops of concentrated acetic acid. The mixture was left in a water bath for 30 min of reaction. This procedure was repeated four times. Then, the mixture was subjected to filtration and drying processes. To calculate the cellulose content, 1 g of biomass was weighed and refluxed with a mixture of 20 ml of acetic acid and methanol in a 1:1 ratio, for 60 min. Subsequently, the sample was cooled and 50 ml of a nitro-alcoholic mixture was added to it. After 60 min of boiling reaction, the mixture was vacuum filtered, washed with deionized water, and dried in an oven at 105 °C until constant weight. Hemicellulose was determined by the difference between the percentage of homocellulose and cellulose. For the determination of lignin, 15 ml of sulfuric acid was added to 1 g of biomass with constant stirring for 2 h. Then, water was added slowly until obtaining a solution with an acid concentration around 3%. The resulting mixture was refluxed for 4 h and allowed to stand for 24 h in order for the insoluble material or lignin to settle completely. Subsequently, the solid was filtered and washed with hot water and dried in an oven at 105 °C until constant weight (Toribio et al. 2014; Watkins et al. 2015; Mansora et al. 2019).

Treatment of the cocoa shell

The cocoa shell was initially subjected to a grinding stage in a TRAPP TRF 300 mill, and subsequently brought to a natural drying stage for 72 h. Then, the ground shell was separated by sieving in a Gran Test—Pinzuar sieve equipment, into three particle sizes with a mesh number ranging between 8 and 120. Subsequently, the crushed cocoa shell called cocoa shell precursor was divided into three groups by particle size intervals for the preparation of three activated carbons, which were coded as A, B, and C.

Chemical activation of biomass

The biomass (cocoa shell precursor) was impregnated with phosphoric acid H_3PO_4 , using impregnation ratio (IR) of 1 and 1.5, between phosphoric acid/cocoa shell (Molina et al. 2004, Lamine et al. 2014; Chen et al. 2017a, b). During the chemical activation stage, approximately 300 g of dry and ground cocoa shell was weighed, and then, H_3PO_4 was added according to the impregnation ratio. The activation of the cocoa shell was carried out with constant stirring, maintaining the temperature at 100 °C for 60 min. The impregnation ratio (IR) can be obtained using Eq. 1:

$$IR = \frac{m_{\text{after impregnation}} - m_{\text{initial}}}{m_{\text{initial}}} \quad (1)$$

where:

m_{initial} = mass of cocoa shell precursor, g.

$m_{\text{sample after impregnation}}$ = mass of biomass after impregnation, g.

m_{liquids} = mass of condensed liquids in the collector during reaction, g.

Thermogravimetric analysis (TGA)

The thermal decomposition was conducted on a thermogravimetric balance (Athlon thermogravimetric analyzer) to 10 mg of previously dried cocoa shell, in the temperature range between 25 and 800 °C, at a heating rate of 15 °C/min with a nitrogen flow of 50 ml/min. To identify the stages of thermal degradation of cocoa shell, the heating rate of 15 °C/min was selected, according to the methodology reported in the literature (Gil et al. 2010).

Pyrolysis testing and experiments design

The activated carbon preparation was realized through a thermochemical process in a Carbolite UN 110 oven, under an inert nitrogen atmosphere at a flow of 20 ml/min (Fig. 1). For each experiment, 300 g of cocoa shell precursor, previously activated with phosphoric acid, was used.

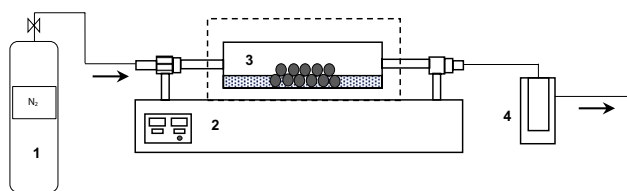


Fig. 1 Scheme of the pyrolysis reactor (Carbolite): 1. nitrogen cylinder, 2. temperature controller, 3. reactor with pellets, 4. liquid collector

The experimental design allows the evaluation of the individual and interaction effect of the factors on the response variable. The 2^k factorial arrangement consists of k factors with two test levels. For example, the effect of k factors can be observed graphically to facilitate the interpretation of the results. The Pareto diagram determines the hierarchy of the main factor. In addition, a large number of tests for each selected factor are not necessary. For the preparation of activated carbons, this work used a 2^3 factorial design to establish the effect of 3 variables: impregnation ratio (IR), temperature, and reaction time, each variable with 2 levels. The responses variables were: surface area and activated carbon yield. Then, the best synthesis conditions in the preparation of the activated carbons A, B, and C were applied. Table 1 shows the three variables and their two levels.

The reaction temperatures were previously determined based on the decomposition results of the thermogravimetry analysis test (Sect. 2.2.4). Subsequently, the activated carbon samples were subjected to a water-based washing process in a Soxhlet extraction system until obtaining washing waters with a pH in the range of 5 to 6. Finally, for the drying process the samples were placed in an oven at a temperature of 105 °C, for 24 h. During the pyrolysis test, the liquid product is condensed in the collector with dry ice. The mass balance was performed by gravimetry, using the following equations:

$$\% \text{ Activated carbon} = \frac{100(m_{\text{final}})}{m_{\text{initial}}} \quad (2)$$

$$\% \text{ Liquids} = \frac{100(m_{\text{liquids}})}{m_{\text{initial}}} \quad (3)$$

$$\% \text{ Gas} = \frac{100(m_{\text{initial}} - m_{\text{final}})}{m_{\text{initial}}} \quad (4)$$

where:

m_{initial} = mass of impregnated sample, g.

m_{final} = mass residual biomass after reaction, g.

m_{liquids} = mass of condensed liquids in the collector during reaction, g.

% Activated carbon = percent by weight of activated carbon after reaction.

% Liquids = percent by weight of liquids after reaction.

Table 1 Factor levels

Factors	Level (-)	Level (+)
X_1 : Temperature (°C)	420	480
X_2 : Impregnation ratio (g shell/g acid)	1	1.5
X_3 : Time (min)	30	120

% gas = percent by weight of gas after reaction.

The best synthesis conditions were used to obtain activated carbons A, B, and C.

Characterization

Surface area determination

The surface area was determined with a Vac Prep 061 Micromeritics equipment. The activated carbon samples were weighed into 9-mm-diameter glass cells and loaded into the equipment. Then, the degassing step was carried out at a temperature of 120 °C, for 2 h. Subsequently, the same procedure was carried out at 300 °C for 10 h, maintaining the vacuum pressure at 6 Pa. The texture characteristics such as surface area and pore volume were determined from adsorption–desorption isotherms with nitrogen at 77 K applying the Brunauer, Emmett, and Teller (BET) method. The specific areas of the samples with the BET method (Brunauer–Emmett–Teller) and the consistency criterion of the Rouquerol transform were calculated (Brunauer et al., 1938; Llewellyn et al. 2017). Nitrogen adsorption in this work was carried out in the range of relative pressure values (p/p°) from 0.02 to 0.99. The information was normalized using 3FLEX V4 software.

ATR-FTIR infrared spectroscopy

The cocoa shell and activated carbons were characterized by ATR-FTIR spectroscopy in order to qualitatively determine the functional groups. The infrared spectra were acquired with a Thermo Scientific Nicolet IS50 FTIR spectrometer, which has an attenuated total reflectance cell equipped with a single-pass diamond reflection crystal, with a 45° fixed angle of incidence. The obtained IR spectra were normalized using the OMNIC software.

Adsorption capacity assessment

Determination of activated carbon adsorption by UV–VIS spectroscopy

Adsorption tests were performed on different solutions of methylene blue and ferric chloride with initial concentrations between 50–450 and 50–350 mg/L, respectively. 0.1 g of activated carbon was added to 5 ml of each solution in 15 ml capped test tubes for centrifuge (Falcon). Subsequently, these tubes were shaken on a FALC F340 Series horizontal shaker, at 150 rpm, for 24 h (estimated time to reach equilibrium). The activated carbon was then separated by centrifugation in a Hettich Zentrifugen 320R equipment

at 6000 rpm for 5 min. The final concentration of methylene blue or ferric chloride was determined from the supernatant liquid.

The methylene blue and ferric chloride calibration curves were estimated in a UV–VIS GO 3.12 spectrophotometer, at $\lambda = 290 \text{ cm}^{-1}$, using solutions in the range of 10 to 125 mg/L, and 10 to 240 mg/L, respectively. Fitting to the calibration correlations was conducted with the Beer–Lambert method.

Adsorption isotherms

- Langmuir model This model assumes that when the adsorbate (methylene blue and ferric chloride) comes into contact with the adsorbent (activated carbon), it only covers the latter with a homogeneous monolayer around its surface. The theoretical model of the Langmuir isotherm proposes that, at equilibrium, the maximum saturation point is obtained when there is no more adsorption in the monolayer formed by the adsorbate. Once a cation occupies an adsorption site, there will be no more molecular attraction at that specific site. The mathematical correlation adjusted to his theory is reflected in Eq. 5 (Basha et al. 2008, Ndi Nsami et al. 2013, Taghdiri et al. 2013, Salahudeen et al. 2014, Wahid et al. 2017):

$$q_e = \left(\frac{q_{\max} \cdot b \cdot C_e}{1 + b \cdot C_e} \right) \quad (5)$$

where q_{\max} and b are the Langmuir constants, which represent the maximum adsorption capacity ($\text{mg} \cdot \text{g}^{-1}$) of the adsorbent, and C_e is the energy constant related to the heat of adsorption ($\text{dm}^3 \cdot \text{mg}^{-1}$). In order to evaluate the parameters b and q_{\max} through the fitted Langmuir isotherms, it is necessary to linearize the model as indicated in Eq. 6:

$$\frac{C_e}{q_e} = \frac{C_e}{q_{\max}} + \frac{1}{q_{\max} b} \quad (6)$$

- Freundlich model This model proposes that the binding sites with the great thermogravimetric test (Fig. 3) attraction force are initially occupied by the adsorbate molecules. Then, the weakest sites are consecutively occupied, thus decreasing the molecular binding as the degree of occupation of each site increases. Freundlich's expression is represented by Eq. 7 (Basha et al. 2008, Ndi Nsami et al. 2013, Salahudeen et al. 2014, Wahid et al. 2017):

$$q_e = k \cdot C_e^{1/n} \quad (7)$$

The adsorption parameters are obtained with Eq. 8,

$$\text{Ln}(q_e) = \text{Ln}(K_f) + \frac{1}{n_f} \text{Ln}(C_e) \quad (8)$$



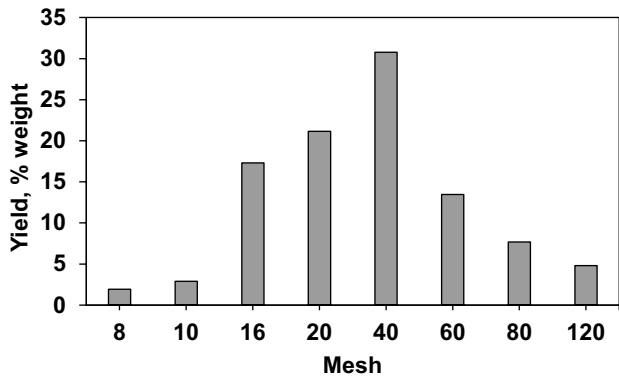
where k_f is the equilibrium constant ($\text{mg}\cdot\text{g}^{-1}(\text{dm}^3\text{mg}^{-1})^{1/n_f}$) and n_f is the constant related to the affinity between the salt (methylene blue or ferric chloride) and the adsorbent (activated carbon).

-- **Temkin isotherm model** This model was developed to understand the indirect effects on the adsorbate–adsorbent interaction. In an isothermal adsorption, the heat of adsorption of all the molecules in the layer decreases linearly (Basha et al. 2008). The adsorption isotherm is represented by Eq. 9 (Basha et al. 2008, Ndi Nsami et al. 2013, Salahudeen et al. 2014, Wahid et al. 2017),

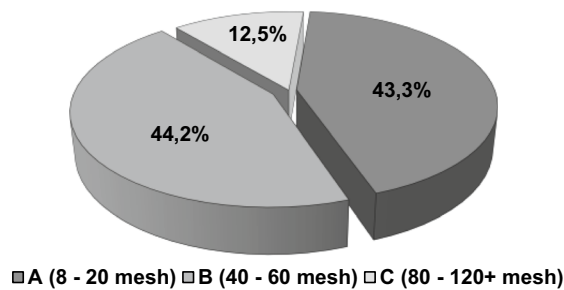
$$q_e = n_T \ln(K_T) + n_T \ln(C_e) \tag{9}$$

where K_T is the Tenkin equilibrium constant, and from n_T it is possible to calculate b , which is related to the heat of adsorption calculated from the expression in Eq. 10:

$$n_T = \frac{RT}{b} \tag{10}$$



(a)



(b)

Fig. 2 Biomass treatment: (a) particle size distribution; and (b) yield distribution by kind of cocoa shell precursor

Results and discussion

Obtaining activated carbons

In this work, cocoa shell-based activated carbon was proposed as a precursor, considering that its high lignin content (28.35% by weight, on a dry basis) is favorable for the performance of the products obtained under pyrolysis conditions. Figure 2a shows the yield by weight of the cocoa shell precursor at different particle diameters after the grinding process.

The ground biomass was divided into three samples by particle size range called cocoa shell precursor A (8–20 mesh), B (40–60 mesh), and C (80–120+ mesh). The weight

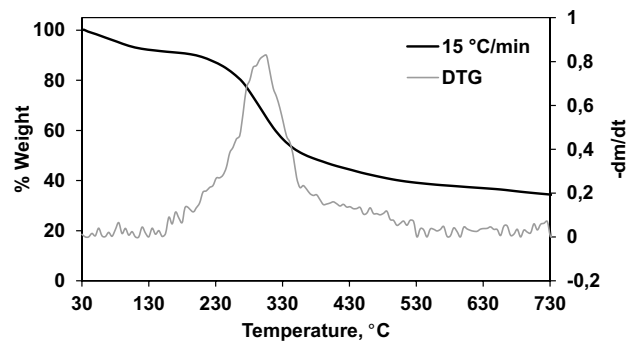
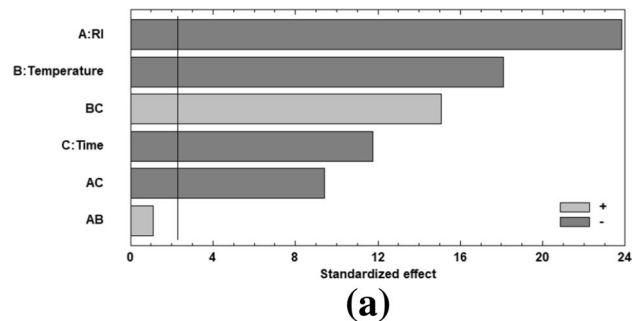
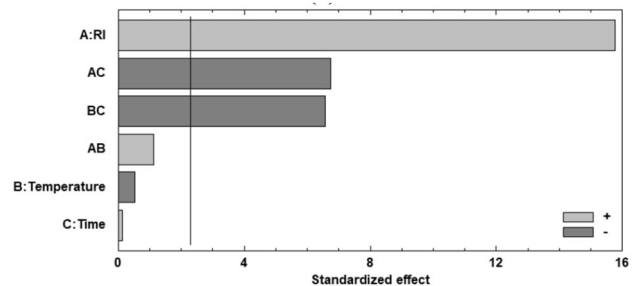


Fig. 3 Cocoa shell thermogram with a heating rate of 15 °C/min



(a)



(b)

Fig. 4 Pareto diagram: (a) activated carbon yield; (b) surface area

percentage of the three cocoa shell samples and the particle size is shown in Fig. 2b. It is concluded that after grinding, the highest percentage is obtained by cocoa shell precursor B, followed by A and the lowest is C.

Figure 3 shows the results of the shell thermogravimetry. Pyrolysis starts at approximately 240 °C. In the DTG curve, a maximum peak associated with the decomposition of cellulose and hemicellulose appears. According to the behavior of the DTG derivative, it can be observed that the greatest mass loss occurs near 310 °C. On the other hand, a cumulative mass loss of 48% by weight is observed around 350 °C, and the mass loss gradient decreases as the temperature increases. The results show that in the range from 400 to 500 °C the mass loss is 8% by weight, achieving a maximum cumulative weight loss of 65% around 700 °C.

Three defined stages are given Fig. 4, the first between 30 and 180 °C where evaporation of light components and water occurs, the second between 200 and 500 °C where the greatest change occurs due to chemical reactions, and the last stage where there is less mass loss due to decomposition reactions. These trends are similar to the results reported by various authors (Garcia et al. 2008; Salahudeen et al. 2014; Carrier et al. 2011; Zhang et al. 2014; Jo et al. 2017; Cai et al. 2018), who determined that hemicellulose and cellulose decompose in the temperature range between 200–260 °C and 240–350 °C, respectively. The increase in temperature causes the breaking of glycosidic bonds and some C—C bonds of the hydrocarbons, alcohols, aldehydes, acids, and others (Wang et al. 2007). However, these compounds tend to generate tar, carbon, and light gases such as CO, CO₂, H₂O, and others. Meanwhile, lignin decomposes at temperatures above 280 °C. Therefore, the multiple reactions give rise to the formation of a carbon-rich product as lignin decomposes at higher temperatures (Gao et al. 2016; Yang et al. 2020). These results corroborate that the cocoa shell precursor used in the present work tends to form solid residues with significant yields around 400 °C.

Analysis of the 2³ factorial experiment

Table 2 reports the product yields of each pyrolysis test used to obtain activated carbons, using the fitting of the maximum and minimum variables values of the experiment design which was performed with the Statgraphics Centurion XVII software.

Table 2 and the Pareto diagram (Fig. 4) show that the yield and the surface area of the activated carbons, obtained from the cocoa shell precursor in the pyrolysis process, depend on the effects of IR > temperature > time, in that order.

Likewise, the chart shows that variables and interactions AC (RI and Time) and BC (Temperature and Time) exceed the statistical limit point of t value (size of the difference between the population's mean), which represents a significant contribution. Meanwhile, the results indicate that the surface area of the activated carbons depends on the impregnation ratio (IR). However, this property does not depend on the levels used for the temperature and time factors. The activated carbon yield increases significantly due to the dehydrating character of phosphoric acid that facilitates the loss of hydrogen and oxygen in the form of water. These reactions produce carbon enrichment and also generate improvement in the textural properties of the adsorbent material. (Gao et al. 2016).

The texture of activated carbon varies in terms of the phosphoric acid ratio and the rotary kiln temperature in the pyrolysis stage. The impregnation ratio is the most important effect, and must be considered before each pyrolysis test in order to obtain carbons with the desired qualities. Activated carbons with high surface area values for conditions of impregnation ratio, temperature, and time are obtained, with values of 1.5, 480 °C, and 30 min, respectively. These process conditions were selected for the prepared activated carbons from cocoa shell precursor with different particle

Table 2 Yield and characterization of cocoa shell pyrolysis products

Sample	RI	Temperature, °C	Time, min	% Activated carbon	% Liquids	% Gas	Surface area (m ² /g)	Pore volume (cm ³ /g)	Pore size (nm)
1	1.5	420	30	32.36	41.33	26.31	1128.00	0.50	5.18
2	1	420	120	32.18	46.84	20.97	963.79	0.31	4.18
3	1.5	480	120	27.80	58.08	14.12	1006.50	0.42	5.02
4	1	480	30	30.35	49.78	19.87	791.67	0.23	4.01
5	1	480	120	31.31	39.03	29.66	730.09	0.21	4.05
6	1.5	480	30	28.20	33.80	38.00	1217.72	0.52	5.09
7	1.5	420	120	28.00	54.42	17.57	1079.58	0.50	5.07
8	1	420	30	34.19	44.84	20.96	626.45	0.21	4.09



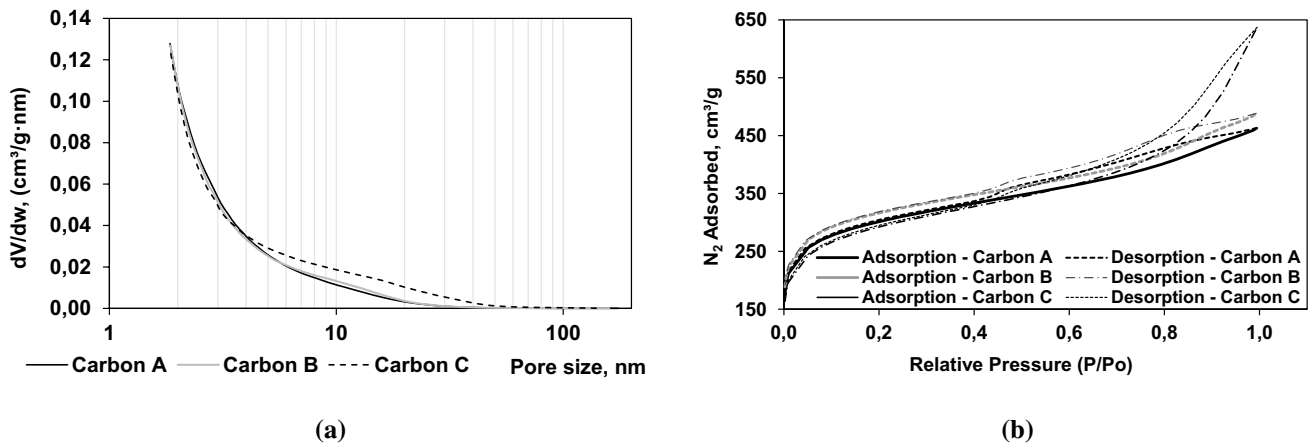


Fig. 5 Surface area. (a) pore size distribution; (b) nitrogen adsorption isotherms

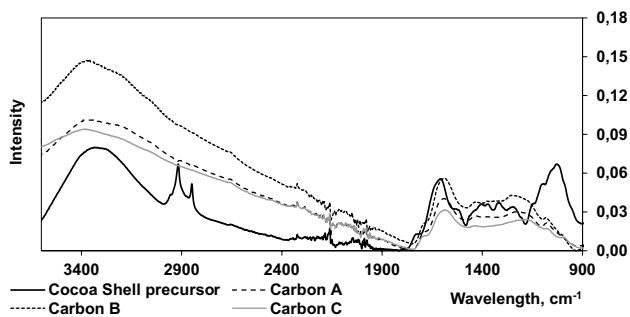


Fig. 6 Infrared spectra of the cocoa shell precursor and its activated carbons

diameters. Subsequently, the carbons in adsorption tests of methylene blue and ferric chloride salts will be applied. Before starting the adsorption studies of the activated carbons, it is necessary to determine their textural and chemical properties, considering that the adsorption efficiency depends on the pore structure. Figure 5a shows the volume distribution by pore type for activated carbons A, B, and C obtained from cocoa shell precursor.

According to IUPAC (International Union of Pure and Applied Chemistry), activated carbons are classified according to their pore size as, macropores (> 50 nm in diameter), mesopores (2–50 nm in diameter), and micropores (< 2 nm in diameter). Therefore, activated carbons A, B, and C present mesoporous structures with values of: 80.68, 80.84, and 81.07%, respectively. So, the macropore and micropore structures fractions for the activated carbons range from 17.71 to 18.11% and between 1.21 and 1.22%. Additionally, the porosity of activated carbons A and B is in the pore size

Table 3 Characterization of the activated carbons surface area

Sample	Surface area (m^2/g)	Pore volume (cm^3/g)	Pore size (nm)
A	990.78	0.39	4.23
B	1217.72	0.52	5.09
C	969.43	0.69	6.66

region between 2 and 30 nm. Meanwhile, carbon C is in the pore size region between 2 and 50 nm.

According to the nitrogen adsorption–desorption behavior, the results show that the activated carbons present a hysteresis cycle, which allows classifying these materials as type IV isotherms of the IUPAC classification (Fig. 6b). However, carbon C shows a higher hysteresis cycle, which indicates that the adsorbent–adsorbate interaction is lower than carbons A and B. In Fig. 5b, is observed the complete formation of the monolayer from the reduced pressure value of approximately 0.06, and after this value, the multilayer adsorption occurs. The results show similar trends to works reported by other authors, where significant nitrogen adsorption is observed at low relative pressures, corresponding to adsorption in micropores (Martín et al. 1990; Puziy et al. 2017). On the other hand, increased adsorption at intermediate and high relative pressures is characteristic of multilayer adsorption formation. Table 3 shows the surface area of the A, B, and C synthesized activated carbons, obtained by pyrolysis of the cocoa shell precursors with mesh particle diameters of 8–20, 40–60, and 80–120+, respectively.

The activated carbons synthesized showed a slight increase in pore volume in the increasing order of $A < B < C$ and the surface areas are around $1000 m^2/g$. That indicates

that the proposed methodology with the factorial design of experiments in the thermochemical treatment on cocoa shell precursor with particle mesh diameters between 8 and 120 μm is suitable to obtain activated carbons with very prominent surface areas.

Characterization of activated carbons by FTIR spectroscopy

Figure 6 shows the infrared spectra of the cocoa shell precursor and its activated carbons. The results of the ATR-FTIR spectra provide unique information about the functional groups present on the activated carbons surface, which are useful to relate the chemical composition with the adsorption properties.

The variation of the peaks in the infrared spectra that the thermochemical test conditions and the particle diameter of the cocoa shell precursor produce different effects on the structure of the activated carbon is evidence.

The broad bands between 3600 and 2900 cm^{-1} are related to the $-\text{OH}$ group, which can be attributed to the presence of surface species such as phenol type and carboxylic acid. The stretch bands between 1550 and 1650 cm^{-1} , corresponding to the $\text{C}=\text{O}$ group, can be mainly attributed to carboxylic

acids. However, functional groups associated with lactones or cyclic ester-type organic compounds are present in this region, and these compounds can overlap at around 1630 cm^{-1} . The bands between 990 and 1300 cm^{-1} , there is an intensity that corresponds to $\text{C}-\text{O}$ type single bonds, both ethers, and hydroxyls.

The FTIR spectrum of the cocoa shell precursor sample shows vibrations of the methylene $>\text{CH}_2$ group typical of cycloalkanes around 1025 cm^{-1} and the $\text{C}-\text{H}$ of methyl groups between 1290 to 1400 cm^{-1} . In addition, bands at 2850–2920 cm^{-1} typical of aliphatic $\text{C}-\text{H}$ stretching and 1375–1465 cm^{-1} associated with aliphatic $\text{C}-\text{H}$ bending, are observed. The results show that the intensities of some characteristics groups present in the cocoa shell precursor are absent in the activated carbons obtained during the thermochemical process at 480 $^{\circ}\text{C}$. Therefore, the decrease in H atoms shows that the activated carbons present structures with high carbon content with graphitized type carbon structural arrangement. The signals attributed in this study corroborate with the results reported in the literature (Fuente et al. 2003; Allwaret et al. 2016; Nandiyanto et al. 2019).

The decrease in intensity in the aliphatic bending and stretching region indicates that activated carbons are mainly composed of aromatic and cyclic oxygen-rich structures typical of phenolic, carboxylic compounds. The results affect that the abundance of these functional groups influences the chemical nature of the surface of each activated carbon. From the normalized spectra, it is observed that the intensities of the bands of these structures are higher for activated carbon B followed by activated carbons A and C. In this case, it is probably due to the oxidation produced by the phosphoric acid.

Methylene blue and ferric chloride adsorption analysis

The calibration curves (concentration vs absorbance) for the methylene blue and ferric chloride solutions are given Fig. 7, using the absorbances measured at $\lambda = 290 \text{ nm}$ (Abs_{λ}),

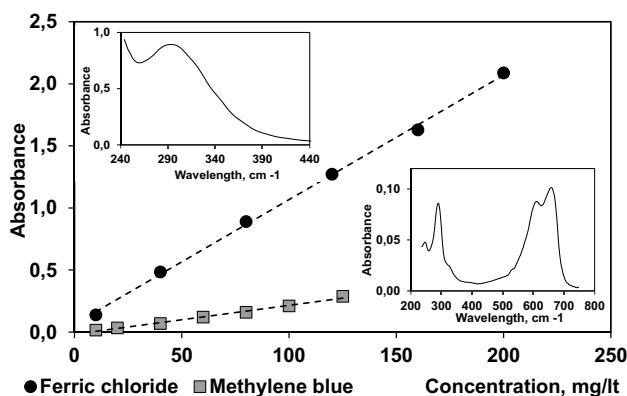


Fig. 7 UV-VIS calibration spectra for salts

Fig. 8 Adsorption behavior of methylene blue in activated carbons: **a** adsorption capacity (q_e) and **b** percent removal efficiency (% RE)

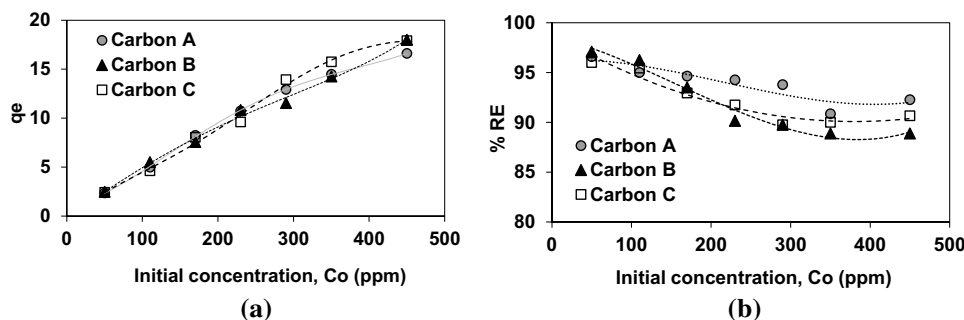


Fig. 9 Adsorption behavior of ferric chloride in activated carbons: **a** adsorption capacity (q_e); and **b** percent removal efficiency (% RE)

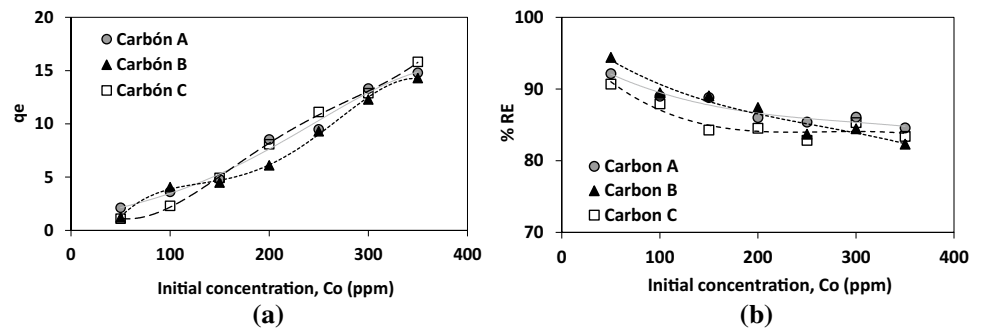
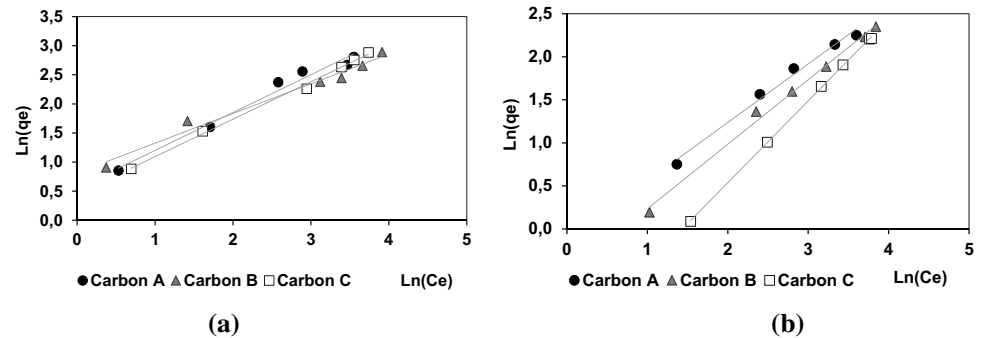


Fig. 10 Freundlich isotherms in activated carbons: **a** methylene blue and **b** ferric chloride



which showed coefficients of determination (R^2) of 0.9801 and 0.9948, respectively.

The correlations obtained from the calibration curves using the Beer–Lambert’s law are shown in Eqs. 11 and 12.

$$\text{Methylene blue} : C_e = 8, .2 + 432.3Abs_\lambda \quad (11)$$

$$\text{Ferric chloride} : C_e = 0.09 + 0.009Abs_\lambda \quad (12)$$

Assessment of the adsorption capacity

The adsorption capacity of methylene blue increases as their initial concentration in the solution increases, for the three carbons studied (Fig. 8). The percent removal tends to decrease with increase in concentration. The results show that the adsorption tendency of methylene blue, for concentrations (C_o) between 50 to 100 mg/L, is in the order of $B > C > A$. For higher concentrations, the adsorption of activated carbons is in the order of $A > C > B$.

The ferric chloride adsorption results (Fig. 9) show similar trends to methylene blue. However, the percent removal of ferric chloride is lower with increase in initial concentration. For concentrations between 50 and 200 mg/L, the carbons are ordered as $B > C > A$. While, for higher concentrations the adsorption order of the activated carbons is ordered as $A > C > B$, keeping the same absorbent ratio.

Figure 10 shows the fitting of the experimental data for the adsorption of methylene blue and ferric chloride

using the Freundlich isotherm for the activated carbons A, B, and C. The results show that at low concentrations of methylene blue and ferric chloride salts, there is a greater removal, but the available sites are occupied as the concentration increases. In addition, results show that activated carbon B has high adsorption efficiency of methylene blue and ferric chloride in the concentration ranges of 50–100 mg/L and 50–200 mg/L, respectively.

The adsorption kinetics parameters for fitting the adsorption behavior of methylene blue and ferric chloride to Langmuir, Freundlich, and Temkin isotherms were calculated by linear regression as shown in Eqs. (6), (8), and (9). The coefficients of determination (R^2) for the Freundlich isotherms are close to 1, and these are greater than the coefficients reported for the Langmuir and Temkin isotherms (Table 4).

Similarly, the sum of squared errors (SSE) parameter of the adsorption tests for methylene blue and ferric chloride shows minimum values for the Freundlich model, followed by the Langmuir and Temkin models, respectively. Thus, the Freundlich isotherm shows a better fit to the experimental adsorption data of methylene blue and ferric chloride, which suggests that monolayer and multilayer adsorption occurred on the surface of activated carbons. The results of the maximum adsorption capacity (q_{max}) of the Langmuir model show that the removal of methylene blue is greater, compared to the ferric chloride salt, in the three activated carbons. On the other hand, the n values for Freundlich isotherms suggest that there exists a greater affinity between methylene blue and the three activated carbons than to the



Table 4 Adsorption kinetics parameters of adsorption isotherms

Carbon	Methylene blue											
	Langmuir				Freundlich				Temkin			
	q_{\max}	b	R^2	SSE	n_F	k_F	R^2	SSE	n_T	K_T	R^2	SSE
A	23.78	0.06	0.96	0.63	1.54	1.73	0.98	1.21	4.72	1.30	0.96	1.61
B	20.10	0.07	0.91	1.18	1.96	2.26	0.98	0.64	3.82	1.09	0.97	0.97
C	26.46	0.04	0.91	0.84	1.55	1.57	0.99	0.37	4.90	1.60	0.93	1.73
<i>Ferric chloride</i>												
A	17.46	0.03	0.99	0.16	1.50	0.91	0.99	0.36	3.34	0.44	0.98	0.45
B	19.96	0.02	0.95	0.3	1.33	0.60	0.99	0.23	2.85	0.45	0.93	0.96
C	18.63	0.01	0.98	1.6	1.05	0.26	0.98	0.08	3.66	0.23	0.93	0.79

ferric chloride salt. Furthermore, the equilibrium constants of the Freundlich and Temkin models show that the adsorption rate is higher for methylene blue.

The results show that the conditions selected with the factorial experimental design allow high performance of the dehydrating character of H_3PO_4 and the decomposition reactions of the carbonaceous structure of the cocoa shell. Therefore, these characteristics produce activated carbons with new pores that increase the surface area and textural properties. In general, the thermochemical treatment employed produces mesoporous activated carbons.

The chemical modification of the activated carbons revealed an increase in the oxygen content present in functional groups associated with carboxylic acids and phenols. The content of these functional groups produced significant changes in the physical properties of the material and the adsorption capacity of adsorbents such as methylene blue and ferric chloride. The results obtained from the characterization of synthesized activated carbons show consistency with the results reported by other researchers (Giraldo et al. 2008; Hesas et al. 2013; Bazan et al. 2016; Priya et al. 2020). The chemistry of the surface depends on the presence of functional groups, and therefore, their nature is fundamental to the adsorption capacity. According to the methodology proposed in this work, activated carbon B which presents greater effectiveness in adsorption capacity is determined. This property to the content of functional groups reported and the textural properties such as surface area, volume, and pore size is attributed. Likewise, the adsorption capacity depends on the nature of the adsorbate.

Conclusion

Cocoa shell-based activated carbons were synthesized with surface areas between 970 and 1200 m^2/g , and the best conditions of temperature, impregnation ratio acid/cocoa shell precursor, and reaction time were 480 °C, 1.5, and 30 min, respectively.

Cocoa shell-based activated carbons, obtained with the phosphoric acid activation method, presented significant amounts of functional groups R–OH, R–COOH, and R–OCO, among others, possibly associated to substances such as phenols, carboxylic acids, lactones, ethers, and esters. Therefore, the high adsorption capacity of activated carbons against the methylene blue and ferric chloride salts is due to the texture of the material and its chemical nature. From the adsorption results, it was evidenced that, for concentrations of methylene blue and ferric chloride in the range of 50–100 mg/l, and 50–250 mg/l, respectively, the efficiency of the three activated carbons follows the order of $B > C > A$.

In general, considering the adsorption kinetics parameters obtained in the adsorption curves using the Freundlich method, the abundance of the functional groups OH, C=O, and -CO, and the surface area of 1217 m^2/g , the carbon activated B has higher adsorption kinetics compared to the methylene blue and ferric chloride salts under study. Therefore, with the methodology proposed in this work, it was possible to synthesize activated carbons with excellent chemical and textural properties.

Acknowledgements The authors remain grateful to the Industrial University of Santander (UIS) and their professionals for the running of research projects.

Funding The authors acknowledge the financial support provided by Department of Santander and the Industrial University of Santander (UIS) through agreement BPIN—201600010046.

Declarations

Conflict of interest No potential conflict of interest was reported by the authors.

References

Afoakwa EO, Quao J, Takrama J, Budu AS, Saalia FK (2013) Chemical composition and physical quality characteristics of Ghanaian

- cocoa beans as affected by pulp pre-conditioning and fermentation. *J Food Sci Technol* 50(6):1097–1105
- Agrawal VR, Vairagade VS, Kedar AP (2017) Activated carbon as adsorbent in advance treatment of wastewater. *IOSR J. Mechan. Civil Eng.* 14:36–40
- Aliakbari Z, Younesi H, Ghoreyshi AA, Bahramifar N, Heidari A (2018) Production and characterization of sewage-sludge based activated carbons under different post-activation conditions. *Waste and Biomass Valoriz.* 9(3):451–463
- Alkathiri DSS, Sabri MA, Ibrahim TH, ElSayed YA, Jumean F (2020) Development of activated carbon fibers for removal of organic contaminants. *Int J Environ Sci Technol* 17(12):4841–4852
- Allwar A (2016) Preparation and Characteristics. *Int J Appl Chem* 12(3):183–192
- Basha S, Murthy ZVP, Jha B (2008) Sorption of Hg(II) from Aqueous Solutions onto *Carica papaya*: Application of Isotherms. *Ind Eng Chem Res* 47(3):980–986
- Bazan A, Nowicki P, Pórolniczak P, Pietrzak R (2016) Thermal analysis of activated carbon obtained from residue after supercritical extraction of hops. *J Therm Anal Calorim* 125(3):1199–1204
- Bhatti ZA, Mahmood Q, Raja IA, Malik AH, Khan MS, Wu D (2011) Chemical oxidation of carwash industry wastewater as an effort to decrease water pollution. *Phys. Chem. of the Earth, Parts a/b/c* 36(9–11):465–469
- Brunauer S, Emmett PH, Teller E (1938) Adsorption of gases in multilayered layers. *J Am Chem Soc* 60(2):309–319
- Cai J, Xu D, Dong Z, Yu X, Yang Y, Banks SW, Bridgwater AV (2018) Processing thermogravimetric analysis data for isoconversional kinetic analysis of lignocellulosic biomass pyrolysis: Case study of corn stalk. *Renew Sustain Energy Rev* 82:2705–2715
- Campos-Vega R, Nieto-Figueroa KH, Oomah BD (2018) Cocoa (*Theobroma cacao* L.) pod husk: Renewable source of bioactive compounds. *Trends Food Sci Technol* 81:172–184
- Carrier M, Loppinet-Serani A, Denux D, Lasnier JM, Ham-Pichavant F, Cansell F, Aymonier C (2011) Thermogravimetric analysis as a new method to determine the lignocellulosic composition of biomass. *Biomass Bioenerg* 35(1):298–307
- Charles J, Bradu C, Morin-Crini N, Sancey B, Winterton P, Torri G, Crini G (2016) Pollutant removal from industrial discharge water using individual and combined effects of adsorption and ion-exchange processes: Chemical abatement. *J Saudi Chem Soc* 20(2):185–194
- Chen R, Li L, Liu Z, Lu M, Wang C, Li H, Wang S (2017) Preparation and characterization of activated carbons from tobacco stem by chemical activation. *J Air Waste Manag Assoc* 67(6):713–724
- Chen L, Wang L, Wu X, Ding X (2017) A process-level water conservation and pollution control performance evaluation tool of cleaner production technology in textile industry. *J Clean Prod* 143:1137–1143
- Contescu CI, Adhikari SP, Gallego NC, Evans ND, Biss BE (2018) Activated carbons derived from high-temperature pyrolysis of lignocellulosic biomass. *C—Journal of Carbon Research* 4(3):51
- Deliyanni EA, Kyzas GZ, Triantafyllidis KS, Matis KA (2015) Activated carbons for the removal of heavy metal ions: A systematic review of recent literature focused on lead and arsenic ions. *Open Chem* 13(1)
- Deng M, Yang X, Dai X, Zhang Q, Malik A, Sadeghpour A (2020) Heavy metal pollution risk assessments and their transportation in sediment and overlay water for the typical Chinese reservoirs. *Ecological Indicators* 112:106166
- Díaz I, Rodríguez M, Arnaiz C, San Miguel G, Dominguez M (2013) Biomass pyrolysis kinetics through thermogravimetric analysis. In *Comp. Aided Chem. Eng.* 32:1–6
- Egirani DE, Poyi NR, Shehata N (2020) Preparation and characterization of powdered and granular activated carbon from Palmae biomass for cadmium removal. *Int J Environ Sci Technol* 17(4):2443–2454
- Fakhru'l-Razi A, Pendashteh A, Abdullah LC, Biak DR, Madaeni SS, bidin ZZ. 2009. Review of technologies for oil and gas produced water treatment. *J Hazard Mater* 170(2–3):530–551
- Fares R, Aissa A, Bouadi A, Lounis, M (2018) Biological Treatment of wastewater by Addition of Activated carbon powder (CAP). *J Waste Recycling* 3(1:2):1–7
- Faria PCC, Órfão JJM, Figueiredo JL, Pereira MFR (2008) Adsorption of aromatic compounds from the biodegradation of azo dyes on activated carbon. *Appl Surf Sci* 254(11):3497–3503
- Fuente E, Menéndez JA, Díez MA, Suárez D, Montes-Morán MA (2003) Infrared spectroscopy of carbon materials: a quantum chemical study of model compounds. *J Phys Chem B* 107(26):6350–6359
- Gao Y, Xu S, Ortoboy S, Kan Y, Yue Q, Gao B (2016) Preparation of well-developed mesoporous activated carbon with high yield by ammonium polyphosphate activation. *J Taiwan Inst Chem Eng* 66:394–399
- García-Núñez JA, García-Pérez M, Das KC (2008) Determination of kinetic parameters of thermal degradation of palm oil mill by-products using thermogravimetric analysis and differential scanning calorimetry. *Trans ASABE* 51(2):547–557
- Gil MV, Casal D, Pevida C, Pis JJ, Rubiera F (2010) Thermal behaviour and kinetics of coal/biomass blends during co-combustion. *Biores Technol* 101(14):5601–5608
- Giraldo L, García V, Moreno JC (2008) Superficial Characterization in Gas and Liquid Phase of Activated Carbons. *Revista De Ingeniería* 27:07–16
- Hameed BH, El-Khaiary MI (2008) Equilibrium, kinetics and mechanism of malachite green adsorption on activated carbon prepared from bamboo by K₂CO₃ activation and subsequent gasification with CO₂. *J Hazard Mater* 157(2–3):344–351
- Han K, Wang Q, Zhao J, Luo KH, Li H, Chen Y, Lu C (2016) Combustion pattern, characteristics, and kinetics of biomass and chars from segmented heating carbonization. *Asia-Pacific J. Chem. Eng.* 11(5):812–822
- Harsha KS, Murthy M, Udayasimha L, Rangappa D (2017) Synthesis and characterization of activated carbon coated alumina as nano adsorbent. *Materials Today: Proceedings* 4(11):12321–12327
- Heiderscheidt E, Leiviskä T, Kløve B (2015) Chemical treatment response to variations in non-point pollution water quality: Results of a factorial design experiment. *J Environ Manage* 150:164–172
- Hesas RH, Arami-Niya A, Daud WMA, Sahu JN (2013) Preparation and characterization of activated carbon from apple waste by microwave-assisted phosphoric acid activation: application in methylene blue adsorption. *BioResources* 8(2):2950–2966
- Igunnu ET, Chen GZ (2014) Produced water treatment technologies. *Int. J. Low-Carbon Technol.* 9(3):157–177
- Jan FA, Ishaq M, Ihsanullah I, Asim SM (2010) Multivariate statistical analysis of heavy metals pollution in industrial area and its comparison with relatively less polluted area: a case study from the City of Peshawar and district Dir Lower. *J Hazard Mater* 176(1–3):609–616
- Jo JH, Kim SS, Shim JW, Lee YE, Yoo YS (2017) Pyrolysis characteristics and kinetics of food wastes. *Energies* 10:1191
- Lamine SM, Ridha C, Mahfoud HM, Mouad C, Lotfi B, Al-Dujaili AH (2014) Chemical activation of an activated carbon prepared from coffee residue. *Energy Procedia* 50:393–400
- Liu F, Zhang Z, Wang Z, Li X, Dai X, Wang L, Wang X, Yuan Z, Zhang J, Chen M, Wang S (2019) Experimental study on treatment of tertiary oil recovery wastewater by electrocoagulation. *Chem. Eng. Process. Process Intensific.* 144:107640
- Llewellyn P, Rodriguez-Reinoso F, Rouquerol J, Seaton N (2007) Characterization of porous solids VII. *Studies in Surface Science and Catalysis*, Eds. (Elsevier, 2007) 160:49–56

- Ma Y (2017) Comparison of activated carbons prepared from wheat straw via ZnCl₂ and KOH activation. *Waste and Biomass Valoriz.* 8(3):549–559
- Manals-Cutiño E, Penedo M, Giralt-Ortega G (2011) Thermogravimetric and thermal analysis differential different vegetable biomasses. *Tecnología Química (cuba)* 31(2):180–190
- Mansora AM, Lima JS, Anib FN, Hashima H, Hoa WS (2019) Characteristics of Cellulose, Hemicellulose and Lignin of MD2 Pineapple Biomass. *Chem Eng Trans* 72:79–84
- Martín MJ (1988) Adsorción Física de Gases y Vapores por Carbones (in Spanish). Universidad De Alicante: Alicante, España 1988:5–40
- Melgar A, Borge D, Pérez JF (2008) Kinetic study of the biomass devolatilization process in particles sizes between 2–19 mm by means of thermogravimetric analysis. *Dyna* 75(155):123–131
- Meng LY, Ma MG, Ji XX (2019) Preparation of lignin-based carbon materials and its application as a sorbent. *Materials* 12(7):1111
- Molina-Sabio M, Rodríguez-Reinoso F (2004) Role of chemical activation in the development of carbon porosity. *Colloids Surf, A* 241(1–3):15–25
- Nandiyanto ABD, Oktiani R, Ragadhita R (2019) How to read and interpret FTIR spectroscopy of organic material. *Indon. J. Sci. Technol.* 4(1):97–118
- Ndi Nsami J, Ketcha MJ (2013) The Adsorption efficiency of chemically prepared activated carbon from cola nut shells by on methylene blue. *J Chem* 2013:1–7
- Ndolomingo MJ, Meijboom R (2015) Kinetic analysis of catalytic oxidation of methylene blue over γ -Al₂O₃ supported copper nanoparticles. *Appl Catal A* 506:33–43
- Odubiyi OA, Awoyale AA, Eloka-Eboka AC (2012) Wastewater treatment with activated charcoal produced from cocoa pod husk. *Int J Environ Bioener* 4(3):162–175
- Oliveira GFD, Andrade RCD, Trindade MAG, Andrade HMC, Carvalho CTD (2017) Thermogravimetric and spectroscopic study (TG–DTA/FT–IR) of activated carbon from the renewable biomass source babassu. *Quim Nova* 40(3):284–292
- Ortiz-R OO, Villamizar Gallardo RA, Rangel JM (2014) Applying life cycle management of colombian cocoa production. *Food Science and Technology* 34(1):62–68
- AO Oyedun TCZ, Hanson S, Hui CW (2014) Thermogravimetric analysis of the pyrolysis characteristics and kinetics of plastics and biomass blends. *Fuel Process Technol* 128:471–481
- Pak SH, Jeon MJ, Jeon YW (2016) Study of sulfuric acid treatment of activated carbon used to enhance mixed VOC removal. *Int Biodeterior Biodegrad.* 113:195–200
- Panahi Y, Mellatyar H, Farshbaf M, Sabet Z, Fattahi T, Akbarzadeh A (2018) Biotechnological applications of nanomaterials for air pollution and water/wastewater treatment. *Mater. Today: Proceed.* 5(7):15550–15558
- Pangeni B, Paudyal H, Inoue K, Kawakita H, Ohto K, Gurung M, Alam S (2014) Development of low cost adsorbents from agricultural waste biomass for the removal of Sr (II) and Cs (I) from water. *Waste and Biomass Valoriz.* 5(6):1019–1028
- Pathania D, Sharma S, Singh P (2017) Removal of methylene blue by adsorption onto activated carbon developed from Ficus carica bast. *Arab J Chem* 10:S1445–S1451
- Priya DS, Sureshkumar MV (2020) Synthesis of Borassus flabellifer fruit husk activated carbon filter for phenol removal from wastewater. *Int J Environ Sci Technol* 17(2):829–842
- Puziy AM, Kochkin YN, Poddubnaya OI, Tsyba MM (2017) Ethyl tert-butyl ether synthesis using carbon catalysts from lignocellulose. *Adsorpt Sci Technol* 35(5–6):473–481
- Rasalingam S, Peng R, Koodali RT (2014) Removal of hazardous pollutants from wastewaters: applications of TiO₂-SiO₂ mixed oxide materials. *J Nanomater* 2014:1–42
- Rivera JA, López VP, Casado RR, Hervás JMS (2016) Thermal degradation of paper industry wastes from a recovered paper mill using TGA. *Characteriz. Gasificat. Test Waste Manag.* 47:225–235
- Robinson T, McMullan G, Marchant R, Nigam P (2001) Remediation of dyes in textile effluent: a critical review on current treatment technologies with a proposed alternative. *Biores Technol* 77(3):247–255
- Salahudeen N, Ajinomoh CS, Nakakana S (2014) Adsorption Isotherm Study for Activated Carbon Produced from Cassava Peel. *J. Mater. Metallurg. Eng.* 4(3):8–12
- Saldarriaga JF, Aguado R, Pablos A, Amutio M, Olazar M, Bilbao J (2015) Fast characterization of biomass fuels by thermogravimetric analysis (TGA). *Fuel* 140:744–751
- Sánchez K, Bacca J, Arévalo-Sánchez L, Arguello H, Castillo S (2021) Classification of Cocoa beans based on their level of fermentation using spectral information. *Tecnológicas* 24(50):172–188
- Shou J, Qiu M (2016) Adsorption of copper ions onto activated carbon from capsicum straw. *Desalin Water Treat* 57(1):353–359
- Sotelo JL, Ovejero G, Rodríguez A, Álvarez S, García J (2013) Analysis and modeling of fixed bed column operations on flumequine removal onto activated carbon: pH influence and desorption studies. *Chem Eng J* 228:102–113
- Taghdiri M, Zamani N (2013) Hexamine adsorption study on activated carbon from aqueous solutions for application in treatment of hexamine industrial wastewater. *Int J Environ Sci Technol* 10(1):19–26
- Tejeda BL, Tejeda TC, Marimón BW, Villabona OÁ (2014) Study of physical and chemical modification of biomass (*Citrus sinensis* and *Musa paradisiaca*) for the adsorption of heavy metals in solution. *Luna Azul* 39:124–142
- Toribio-Cuaya H, Pedraza-Segura L, Macías-Bravo S, Gonzalez-García I, Vasquez-Medrano R, Favela-Torres E (2014) Characterization of lignocellulosic biomass using five simple steps. *J Chem Biol Physic Sci* 4(5):28–47
- Valério Filho A, Xavaré Kulman R, Vaz Tholozan L, Felkl de Almeida AR, Silveira da Rosa G (2020) Preparation and characterization of activated carbon obtained from water treatment plant sludge for removal of cationic dye from wastewater. *Processes* 8(12):1549
- Vuppaladadiyam AK, Liu H, Zhao M, Soomro AF, Memon MZ, Dupont V (2019) Thermogravimetric and kinetic analysis to discern synergy during the co-pyrolysis of microalgae and swine manure digestate. *Biotechnol Biofuels* 12(1):170
- Wahid F, Mohammadzai IU, Khan A, Shah Z, Hassan W, Ali N (2017) Removal of toxic metals with activated carbon prepared from *Salvadora persica*. *Arab J Chem* 10:S2205–S2212
- Wang S, Liu Q, Luo Z, Wen L, Cen K (2007) Mechanism study on cellulose pyrolysis using thermogravimetric analysis coupled with infrared spectroscopy. *Front Energy Power Eng Chin* 1(4):413–419
- Wang S, Guo X, Wang K, Luo Z (2011) Influence of the interaction of components on the pyrolysis behavior of biomass. *J Anal Appl Pyrol* 91(1):183–189



- Wang Q, Xie Z, Li F (2015) Using ensemble models to identify and apportion heavy metal pollution sources in agricultural soils on a local scale. *Environ Pollut* 206:227–235
- Watkins D, Nuruddin M, Hosur M, Tcherbi-Narteh A, Jeelani S (2015) Extraction and characterization of lignin from different biomass resources. *J Market Res* 4(1):26–32
- White JE, Catallo WJ, Legendre BL (2011) Biomass pyrolysis kinetics: a comparative critical review with relevant agricultural residue case studies. *J Anal Appl Pyrol* 91(1):1–33
- Wołowicz M, Komorowska-Kaufman M, Pruss A, Rzepa G, Bajda T (2019) Removal of heavy metals and metalloids from water using drinking water treatment residuals as adsorbents: a review. *Minerals* 9(8):487
- Yakout SM, El-Deen GS (2016) Characterization of activated carbon prepared by phosphoric acid activation of olive stones. *Arab J Chem* 9:S1155–S1162
- Yang Z, Gleisner RH, Mann D, Xu J, Jiang J, Zhu JY (2020) Lignin based activated carbon using H₃PO₄ activation. *Polymers* 12(12):2829
- Yousef R, Qiblawey H, El-Naas MH (2020) Adsorption as a process for produced water treatment: a review. *Processes* 8(12):1657
- Zhang J, Feng L, Wang D, Zhang R, Liu G, Cheng G (2014) Thermogravimetric analysis of lignocellulosic biomass with ionic liquid pretreatment. *Biores Technol* 153:379–382

